Title

Deficiency of C-X-C chemokine receptor type 5 (CXCR5) gene causes dysfunction of retinal pigment epithelium cells.

Journal

Laboratory Investigation, 101(2)

Authors

Lennikov, Anton
Mukwaya, Anthony
Saddala, Madhu
et al.

Publication Date

2021-02-01

DOI

10.1038/s41374-020-00491-4

Peer reviewed

HHS Public Access

Author manuscript

Lab Invest. Author manuscript; available in PMC 2023 July 08.

Published in final edited form as:

Lab Invest. 2021 February ; 101(2): 228–244. doi:10.1038/s41374-020-00491-4.

Deficiency of C-X-C chemokine receptor type 5 (CXCR5) gene causes dysfunction of retinal pigment epithelium cells

Anton Lennikov[1], **Anthony Mukwaya**[2], **Madhu Sudhana Saddala**[1], **Hu Huang**[1]

[1]Department of Ophthalmology, University of Missouri School of Medicine, Columbia, MO, USA

[2]Department of Ophthalmology, Institute for Clinical and Experimental Medicine, Faculty of Health Sciences, Linköping University, Linköping, Sweden

Abstract

Homeostasis of the retinal pigment epithelium (RPE) is essential for the health and proper function of the retina. Regulation of RPE homeostasis is, however, largely unexplored, yet dysfunction of this process may lead to retinal degenerative diseases, including age-related macular degeneration (AMD). Here, we report that chemokine receptor CXCR5 regulates RPE homeostasis through PI3K/AKT signaling and by suppression of FOXO1 activation. We used primary RPE cells isolated from CXCR5-deficient mice and wild type controls, as well as ex vivo RPE–choroidal–scleral complexes (RCSC) to investigate the regulation of homeostasis. CXCR5 expression in mouse RPE cells was diminished by treatment with hydrogen peroxide. Lack of CXCR5 expression leads to an abnormal cellular shape, pigmentation, decreased expression of the RPE differentiation marker RPE65, an increase in the undifferentiated progenitor marker MITF, and compromised RPE barrier function, as well as compromised cell-to-cell interaction. An increase in epithelial-mesenchymal transition (EMT) markers (αSMA, N-cadherin, and vimentin) was noted in CXCR5-deficient RPE cells both in vitro and in age-progression specimens of $CXCR5^{-/-}$ mice (6, 12, 24-months old). Deregulated autophagy in CXCR5-deficient RPE cells was observed by decreased LC3B-II, increased p62, abnormal autophagosomes, and impaired lysosome enzymatic activity as shown by GFP-LC3-RFP reporter plasmid. Mechanistically, deficiency in CXCR5 resulted in the downregulation of PI3K and AKT signaling, but upregulation and nuclear localization of FOXO1. Additionally, inhibition of PI3K in RPE cells resulted in an increased expression of FOXO1. Inhibition of FOXO1, however, reverts the degradation of ZO-1 caused by CXCR5 deficiency. Collectively, these findings suggest that CXCR5 maintains PI3K/AKT signaling, which controls FOXO1 activation, thereby regulating the expression of genes involved in RPE EMT and autophagy deregulation.

✉Hu Huang, huangh1@missouri.edu.

Author contributions The study was conceived and designed by AL and HH; AL, AM, and HH performed primary RPE cell isolation and culture, in vitro experiments, RPE–Choroid–Sclera Complex Flat Mounts staining and analysis. The manuscript writing and figure design were performed by AL, AM, MSS, and HH. All authors reviewed and accepted the final version of the manuscript.

Conflict of interest The authors declare that they have no conflict of interest.

Ethics approval All experiments were approved by the Institutional Animal Care and Use Committee of the University of Missouri School of Medicine (protocol number: 9520) and were in accordance with the guidelines of the Association for Research in Vision and Ophthalmology Statement for the use of animals in ophthalmic and vision research.

Supplementary information The online version of this article (https://doi.org/10.1038/s41374-020-00491-4) contains supplementary material, which is available to authorized users.

Introduction

The retinal pigment epithelium (RPE) is a highly polarized, pigmented, and postmitotic epithelial cell monolayer that offers barrier function and with immune cell properties. RPE cells support the longevity and functionality of photoreceptors via a multitude of functions, such as the retinoid metabolism (visual cycle) and photoreceptor outer segment phagocytosis. However, RPE cell dysfunction plays a central role in various retinal degenerative diseases, including age-related macular degeneration (AMD). Given the dual roles of the RPE in both retinal health and disease, maintenance of RPE cell homeostasis is critical for the health and proper function of the retina. A substantial amount of research has been conducted to determine the molecular and cellular basis of RPE cell death or degeneration [1, 2]. However, many questions remain unanswered; for example, how is homeostasis maintained and regulated in RPE cells? RPE cells can change their properties to adopt those of different cell types, such as neurons, under certain stimuli. As an example, Ma et al. reported a successful reprogramming of RPE cells to retinal neurons by overexpression of (sex-determining region Y)-box 2 [3]. Oxidative phosphorylation and increased generation of reactive oxygen species can cause RPE de-differentiation and hypertrophy; these changes in RPE cell functions are followed by impaired visual function and photoreceptor degeneration elicited by protein kinase B (AKT)/mammalian target of the rapamycin pathway (mTOR) [4]. In addition, metabolic reprogramming, autophagy function, and phagosome maturation play pivotal roles in the maintenance of RPE epithelial characteristics and normal functions under normal conditions both in vivo and in vitro [5–7]. Therefore, understanding how RPE cells maintain their epithelial phenotypic status and normal function is vital for the design of therapeutic interventions.

Initially discovered in 1992 as Burkitt's lymphoma receptor 1 [8], CXCR5 (also known as CD185) is a seven-transmembrane G protein-coupled receptor (GPCR) protein. Binding of CXCR5 to the CXCL13 ligand activates several intracellular singling transduction pathways, including phosphoinositide 3-kinase (PI3K)/AKT, mitogen-activated protein kinase (MEK)/extracellular-signal-regulated kinase 1 (ERK1), and epidermal growth factor (EGF)/ras-related C3 botulinum toxin substrate (Rac), which are essential for cell survival, proliferation, and migration, respectively [9]. CXCR5 is essential for naïve B-cell migration to and maturation in the lymph nodes and spleen, as well as for cluster of differentiation 4 T-cell (T_{FH} and T_{CM}) homing and interaction with B cells. CXCR5, therefore, plays a critical role in immunological responses, such as in lymphocyte maturation and tissue homeostasis [10]. Because the CXCR5/CXCL13 signal axis regulates cell migration and immune responses, it has vital roles in the metastasis of various cancers and the interaction between resident (cancer) cells and infiltrated (immune) cells [11–13]. For example, CXCR5 overexpression in mesenchymal stromal cells can enhance their migration and engraftment into the injured tissue and their immunomodulatory effects [14].

Limited reports exist regarding the role of CXCR5 signaling in retinal disease. Wong et al. reported an aging-dependent increase in the expression of CXCL13 (the ligand of CXCR5) in retinal microglial cells [15]. In a more recent report, an elevated level of CXCR5 protein was found in the aqueous humor of AMD patients [16]. Similarly, we previously reported the increased expression of CXCR5 in the RPE/choroid and the retinal

tissue of elderly mice when compared to young controls [17]. These aged CXCR5$^{-/-}$ mice develop RPE abnormalities, retinal degeneration (RD), and AMD-like phenotypes [17, 18]. We also generated CXCR5/NRF2 double knockout (DKO) mice, characterized their retinal phenotypes, and identified the presence of RD and AMD-like pathological features at an early age (2–6 months) [19]. AMD-like phenotypes in CXCR5-deficient mice are very robust, and they include a loss of the RPE tight junction zonula occludens-1 (ZO-1) protein and sub-RPE accumulation of lipofuscin (A2E), immunoglobulin G (IgG), and several AMD-associated proteins: apolipoprotein E, α-crystallin B, β-amyloid, and complement (C)5b–9 [19].

Recent whole transcriptome analysis of the CXCR5-deficient RPE cells revealed multiple differentially expressed genes (DEGs) involved in PI3K-Akt signaling, mTOR signaling, FoxO, focal adhesion, endocytosis, TNFα-NF-kB Signaling, autophagy, epithelial-mesenchymal transition (EMT), and others [20]. An increased expression of pro-inflammatory factors COX-2 and CCL2 was observed in the RNA isolated from CXCR5-deficient RPE cells.

In the present study, primary RPE cells were derived from C57BL wild-type (WT) and CXCR5$^{-/-}$ (KO) mice and the mechanisms by which CXCR5 exerts protective effects on the RPE were investigated. It was noted that CXCR5 deficiency negatively affects RPE cell functions by impairing epithelial integrity and autophagy, resulting in EMT. In addition, inhibition of PI3K upregulated FOXO1, whose inhibition reverts the CXCR5 deficiency-induced degradation of ZO-1 protein. The presented results suggest that CXCR5 is necessary for maintaining the RPE's epithelial phenotype, and thus essential for normal functionality via maintaining PI3K/AKT signaling and preventing FOXO1 activation.

Results

CXCR5 expression in RPE cells is suppressed by H_2O_2 and by pro-inflammatory stimulation

Histological sections of 5-month-old C57BL6-WT and CXCR5 KO mice eyes were used to examine whether RPE cells express CXCR5. Immunofluorescent (IF) staining showed that CXCR5 was expressed in the RPE layer. However, the clarity of the results was affected due to the strong auto-fluorescence emitted from the nearby photoreceptor segment layers (Fig. S1). To circumvent this issue, we next applied the IHC 3,3′-diaminobenzidine (DAB) staining method. However, the pigmentation of the RPE and choroid layers obscured the DAB signal (Fig. 1a). Therefore, the melanin depigmentation process of the RPE and choroid was performed by incubation of the histological sections in 10% hydrogen peroxide (H_2O_2) for 120 min at 65 °C as described by Manicam et al. [21]. The successfully depigmented samples (Fig. 1b) were stained with DAB using a standard protocol and anti-CXCR5 antibody (ab). The CXCR5 DAB staining signals were present predominantly in the RPE layer in the 5-month-old WT retina and weakly in the Bruch's membrane and choroid (Fig. 1c). The specificity of the staining was further validated by staining the age-matched CXCR5 KO depigmented section with CXCR5 ab; only weak, non-specific background signals were detected (Fig. 1d). The expression of CXCL13 in the primary

WT RPE cells and its extracellular presence in the cell culture media was confirmed by immunofluorescence and dot immunoassay (Fig. S2).

Oxidative stress is a significant pathological factor in RPE degeneration that contributes to AMD development. Here, we investigated the effect of CXCR5 deficiency on RPE sensitivity to oxidative damage. Confluent primary RPE cell cultures derived from the KO and WT mice were treated with 1 μM of H_2O_2. Phosphate-buffered saline (PBS) was used as the control, and the cultures were incubated for 12 h. The cell culture media were collected and used for the lactate dehydrogenase (LDH) cytotoxicity assay. H_2O_2 treatment caused a significant ($p < 0.001$) increase in the LDH release from $CXCR5^{-/-}$ KO RPE cultures compared with the WT cells (Fig. 1e). Next, we examined whether oxidative stress can alter CXCR5 expression in RPE cells. The WT primary RPE cell cultures had been treated with PBS as the control or H_2O_2, and these cells were used for IF staining and western blot (WB) analyses. Treatment with H_2O_2 diminished expression of CXCR5 (Fig. 1f); WB analysis further confirmed these results (Fig. 1g). Quantification of the WB results confirmed a significant difference between the control and the treatment groups (Fig. 1h). The suppressed expression of CXCR5 due to oxidative stress suggests that CXCR5 is essential for RPE homeostasis and function under high-stress conditions.

De-differentiation of the primary CXCR5-deficient RPE cells

To determine the role of CXCR5 in RPE cells, we cultured primary RPE cells isolated from CXCR5 KO and C57BL6-WT mice. Cells were confluent after 4 weeks of culture and were used for the WB analysis, which revealed a significantly ($p < 0.05$) higher expression of both the 45 ($p < 0.05$) and 75 kDa ($p < 0.05$) isoforms of undifferentiated RPE progenitor marker microphthalmia-associated transcription factor (MITF) in the CXCR5 KO RPE cells compared to the WT cells (Fig. 2a, b). Furthermore, a lower expression of the RPE differentiation marker RPE-specific 65 kDa protein (RPE65) was noted in KO RPE cells compared to those from WT mice (Fig. 2c, d). These results suggest that CXCR5-deficient RPE cells lose RPE characteristics and undergo less differentiation or maturation.

The impaired barrier function of the CXCR5-deficient RPE cells

Several approaches were used to investigate whether RPE de-differentiation due to CXCR5 deficiency leads to impaired RPE monolayer formation and to barrier dysfunction. The primary cell cultures derived from CXCR5 KO and C57BL6-WT mice were seeded on electrical cell-impedance sensing (ECIS) cultureware and monitored for transepithelial resistance (TER) using the ECIS system in real-time for 50 h. TER values were consistently and significantly ($p < 0.01$) lower for the CXCR5-deficient KO RPE compared to the WT cells (Fig. 3a). Both RPE cell populations were grown on six-well plates, harvested, and lysed for WB analysis. WB revealed a significantly ($p < 0.01$) lower expression of ZO-1 in the KO cell lysates compared to the WT cells (Fig. 3b, c). In addition, RPE cells from KO and WT mice were cultured on the surface of 44-μm cellulose membranes for 4 weeks, according to a modified protocol [22]. The cells were then subjected to double immunostaining for RPE65 and ZO-1. KO RPE cells produced an incomplete monolayer characterized by poor intercellular connections, disrupted RPE65 organization, abnormal cellular shape, poor cell-to-cell interactions, and prominent voids (indicated by arrows; Fig.

3d). With the supporting cellulose substrate, however, the WT RPE cells demonstrated prominent differentiation, as evidenced by the increased expression and intracellular organization of RPE65, the larger cell size, and the strong ZO-1 expression at cell-to-cell interaction sites (Fig. 3e). These results unequivocally demonstrate that CXCR5 is required for the formation of an integral RPE monolayer and that CXCR5 KO consequently leads to compromised RPE monolayer formation, which is consistent with our previous in vivo observations in CXCR5 KO mice [18, 19]. Consistent with IF observations in Fig. 3d, e, scanning electron microscopy (SEM) imaging revealed defects within the intercellular junctions of KO RPE cells (Fig. 3f) with areas of space between the cells (indicated by arrows), but strong integral connections in the WT RPE cells (Fig. 3g). High-magnification SEM images are presented in Fig. S3.

Increased epithelial-mesenchymal transition in CXCR5-deficient RPE cells

Next, we investigated whether CXCR5 deficiency causes EMT of the RPE cells. To address this question, we examined changes in the expression of the three EMT markers N-cadherin, α-smooth muscle actin (αSMA), and vimentin. We observed that levels of N-cadherin (Fig. 4a–d; $p < 0.001$), αSMA (Fig. 4e–h; $p < 0.001$), and vimentin (Fig. 4i–l; $p < 0.01$) increased in CXCR5 KO RPE cells compared to WT RPE cells. Both WB and IF staining results consistently revealed higher protein levels of the three EMT markers in the KO RPE cells compared to the WT cells. The vimentin-stained RPE cells from the CXCR5 KO mice demonstrated non-RPE cell features with multiple cellular processes (Fig. 4i). These results were further confirmed in age-progression specimens collected from 6, 12, and 24-month-old (m.o.) CXCR5 KO and WT mice by RPE–choroid–sclera complex (RCSC) flat-mount immunostaining for N-cadherin (Fig. 5a, b), αSMA (Fig. 5c, d), and vimentin (Fig. 5e, f). With the apparent increase of abundance and change of RPE cell shape that is most prominent in 24-m.o. animals. Furthermore, RPE cell shape is also abnormal, with most prominent in 24-m.o. CXCR5 KO animals which are consistent with our in vitro observation. In WT animals, αSMA mainly not present, and N-cadherin and Vimentin upregulate in RPE cell-to-cell interaction sites with age that may bear compensatory function. These data corroborate the previously mentioned observations and indicate the requirement of CXCR5 for the epithelial phenotype of RPE cells, thereby suggesting that the phenomenon of the RPE EMT was caused by CXCR5 deficiency.

Deregulated autophagy function of CXCR5-deficient RPE cells

We further investigated whether CXCR5 KO deficiency impacts RPE autophagy by determining the abundance of the following autophagosome proteins: microtubule-associated protein 1A/1B light chain 3B (LC3), its lipid-modified form LC3-II, and the ubiquitin-binding protein p62 (P62). P62 is an autophagosome cargo protein that binds to target proteins, selects them for autophagy, and accumulates in the presence of any type of autophagy impairment. We chose these markers as the interaction pair, where P62 interacts with amino acids Phe 52 and Leu53 present in the hydrophobic binding interface of LC3. Impaired autophagy manifests as a decrease in the LC3B-II isoform as well as the accumulation of P62 [23]. IF staining consistently showed a lower expression of bulk LC3 protein in the cytoplasm in the KO RPE cells (Fig. 6a, b) as well as cytoplasmic accumulation of P62 in CXCR5-deficient RPE cells (Fig. 6c, d). The WB analysis with

LC3 antibody detected the two proteins isoforms LC3B-I and LC3B-II from both KO RPE and WT control on WB (Fig. 6i). LC3B-II isoform was decreased in KO RPE cells, further confirmed by densitometry analysis (Fig. 6e; $p < 0.05$). From the transmission electron microscopy (TEM) images, a high number of phagocytic vesicles (yellow arrows) were noted in the KO RPE cells than in the WT cells (Fig. 6g, h, k; $p < 0.01$). Following lead citrate staining and examined at high magnification, and increased electron absorption of substances within the autophagosome was noted, which is indicative of incomplete degradation by phagosomes in the KO RPE cells, but not in WT RPE cells (Fig. 6i, j). It was also noted that the membrane structures and shapes of the remnants in the KO RPE phagolysosomes resembled mitochondria, potentially suggesting an impaired mitophagy function (Fig. 6i). Next, we transfected KO and WT RPE cells with GFP-LC3-RFP-LC3ΔG, a fluorescent probe to evaluate autophagy as described in the literature [24]. The protein construct produced by the probe is cleaved with endogenous ATG4 proteases into equimolar amounts of GFP-LC3 and RFP-LC3ΔG. GFP-LC3 is degraded by autophagy, while RFP-LC3ΔG remains in the cytoplasm, serving as an internal control. Twenty-four hours after transfection, the GFP signals in CXCR5-deficient RPE cells remained prominent (Fig. 6l) were in WT RPE cells marked decrease of GFP signal was observed (Fig. 6m). Quantification of fluorescent signals and determining the GFP/RFP ratio demonstrated a significantly increased ratio in KO RPE cells (Fig. 6n; $p < 0.001$).

Evaluation of phagocytosis with pHrodo Green Zymosan Bioparticles conjugate

To investigate the phagocytic and lysosomal function of RPE cells, we incubated KO and WT RPE cultures with pHrodo Green tagged zymosan bioparticles conjugate. This probe produces a 488 nm excitation peak fluorescence after being incorporated into the cytoplasm where it is subjected to lysosomal enzyme digestion or degradation. Particles remaining in the culture media are non-fluorescent. Observation of the live cultures indicated that both KO (Fig. 6o) and WT (Fig. 6p) cells showed uptake of the zymosan particles. However, after 48 h of incubation, the intense green fluorescence and visible structure of the particulates were observed in the KO RPE. In the WT RPE, the fluorescent signal declined, and the structure of the particle shape becomes unclear (white arrows) suggestive of particle digestion/degradation. Furthermore, in KO RPE, many cells become strongly fluorescent, rounded, and detached from the substrate. The addition of propidium iodide (PI) to the culture media verified the death of highly zymosan-positive rounded floating cells (yellows signals). Quantification of the zymosan/PI-positive cell numbers demonstrated a significant increase of dead RPE cells overwhelmed with zymosan particles ($p < 0.01$) in where in WT RPE, only a few such cells were observed (Fig. 6q).

Mitochondrial abnormalities of the CXCR5-deficient RPE cells

Additional TEM images demonstrated increased numbers of mitochondria in the cytoplasm of CXCR5 KO RPE relative to WT control cells (Fig. S4A, B, E; $p < 0.01$). High magnification images (Fig. S4C, D) exhibited the disrupted mitochondrial structure (cyan arrows) of the KO RPE, which is in contrast to the integral mitochondria in the WT RPE. These findings are further supported by the abundance of two mitochondrial membrane markers: TOM20 and ATP5A [25] in primary RPE cells from KO and WT mice. WB results revealed higher levels of the two proteins in the KO RPE cells than in the WT control

cells (Fig. S4F, I) and densitometry analysis (Fig. S4G, H) further confirmed its significant increase of TOM20 ($p < 0.01$) and ATP5A ($p < 0.001$) in KO RPE cells, compared with WT. These findings may be suggestive of metabolic changes associated with the absence of CXCR5 and EMT in the RPE cells or changes in the numbers of mitochondria (i.e., by the mitophagy impairment). Further experiments are required for a full elucidation of the metabolic activity of CXCR5 KO RPE cells and a definitive answer to whether the mitochondrial marker protein accumulation is associated with impaired mitophagy, or an actual change in the CXCR5 KO RPE cell energy metabolism profile, or both.

FOXO1 acts as a downstream target of PI3K/AKT and mediates the effect of CXCR5 in RPE cells

We next investigated whether FOXO1 acts as a downstream target of PI3K/AKT and mediates the effect CXCR5 in RPE cells. To address this question, we first analyzed the protein expression of PI3K, AKT, and forkhead box protein O1 (FOXO1) in CXCR5 KO RPE cells and WT RPE cells. Decreased expression levels of PI3K ($p < 0.001$) and AKT ($p < 0.001$) were observed in the KO RPE cells compared with the WT cells, as shown by the IF staining and WB results (Fig. 7a–d). In contrast, the expression of FOXO1 was significantly higher in the KO RPE cells than it was in the WT cells (Fig. 7e, f). Predominant nuclear localization of FOXO1 proteins was revealed by IF staining of the KO RPE cells (Fig. 7g), but the FOXO1 signal intensity was dramatically reduced in the nuclei of WT cells (Fig. 7h). These results indicate that CXCR5 deficiency causes increased expression of FOXO1 and nuclear localization in RPE cells. It has been previously shown that PI3K/AKT negatively regulates FOXO1 [26]; thus, the increased FOXO1 expression and nuclear localization observed here may be due to the suppression of PI3K and AKT. To explore this possibility, primary mouse RPE cell cultures were treated with the CXCR5 ligand or agonist CXCL13 (100 ng/ml). The treatment resulted in a significant decrease of FOXO1 ($p < 0.05$) abundance (Fig. 7i, j). However, the inhibition of PI3K with LY294002 (25 μM) abolished the effect of CXCL13, resulting in a significant ($p < 0.05$) increase of FOXO1 (Fig. 7i, j). Furthermore, the inhibition of the FOXO1 with AS1842856 has significantly improved the expression of ZO-1 in CXCR5-deficient RPE cells relative to WT control cells. Interestingly, CXCL13 (100 ng/ml) treatment also significantly increased proliferation ($p < 0.001$) of mouse RPE cells as evaluated by bromodeoxyuridine (BrdU) incorporation enzyme-linked immunosorbent assay (ELISA) assay (Fig. 7m), but the increased activity was abolished by inhibition of PI3K with LY294002 (25 μM).

Deposition of AMD-associated proteins to cellulose substrate of primary mouse CXCR5$^{-/-}$ RPE cells

Our recent mouse studies have confirmed that CXCR5-deficient animals demonstrate the increased presence of β-amyloid and APOE in the RCSC. However, the exact cellular source of these proteins have remained unclear [18]. Therefore, we investigated the effect of CXCR5 deficiency on the extracellular deposition of AMD-associated proteins in primary mouse RPE cultures, using the method previously described by Jonhson et al. [22]. The extracellular depositions of β-amyloid (Fig. 8a) and APOE (Fig. 8c) was observed at a depth of 3–5 μm underneath the Calcein AM-visualized cell border in CXCR5 KO RPE cells. There was no similar deposition evident in WT RPE cells (Fig. 8b, d).

Discussion

This study illustrates the homeostatic role of CXCR5 signaling in RPE cells. We explicitly showed that RPE cells express CXCR5 and CXCL13 in the autocrine fashion, consistent with our previous report of increased CXCL13 presence in RCSC complexes of adult [19] and aged [18] CXCR5 KO mice and a substantial increase in CXCR5/NRF2 DKO animals [19]. CXCR5 expression is also reduced in the oxidative stress environment. Using primary RPE cells in culture derived from WT and KO mice, we found that CXCR5 is required for the maintenance of the RPE's phenotype and function. In primary culture, CXCR5-deficient RPE cells have various cellular dysfunctions, including de-differentiation, compromised barrier function, and autophagy deregulation. The proliferation of RPE cells on a cellulose substrate further aggravated the existing cellular monolayer deficiency, which was suggestive of collagen systems/extracellular matrix deficiency that is supported by our recent whole transcriptome analysis of primary RPE cells where DEGs related to these pathways were significantly downregulated [20]. EMT transformation of RPE cells was further confirmed by ex vivo immunofluorescent analysis of EMT markers in RCSC of adult and aged CXCR5-deficient mice.

We suggest that the PI3K/AKT/FOXO1 signaling axis might be the underlying pathway that mediates the role of CXCR5 in RPE cells. Our findings support the theory that CXCR5 maintains RPE homeostasis via maintenance of PI3K/AKT signaling and suppression of FOXO1 activation in WT RPE cells. Consequently, CXCR5 deficiency leads to RPE EMT, autophagy deregulation, mitochondrial dysfunction, and finally, RD via FOXO1 transcription activation due to impaired PI3K/AKT signaling in KO RPE cells that are associated with extracellular deposition of AMD-associated proteins. This hypothesis is corroborated by the additional data that recombinant protein CXCL13 (the CXCR5 ligand) reduced the FOXO1 protein level, which was reverted by PI3K inhibition (Fig. 7i, j) and that the ZO-1 degradation in CXCR5 KO RPE can be rescued by FOXO1 inhibitor AS1842856. Together, our data support that contention the PI3K/AKT signaling pathway mediates CXCR5 control of FOXO1 expression and downstream effect on RPE, such as ZO-1 degradation.

The bulk of the previous literature shows that CXCR5 plays a vital role in the immune response, tissue homeostasis, and cancer metastasis. Recently, we demonstrated the anti-inflammatory role of CXCR5 in retinal ischemia [27]. The downstream transduction pathway of the CXCR5/CXCL13 signaling axis, such as PI3K/AKT, MEK/ERK1, and EGF/Rac, are implicated in cell survival, proliferation, and migration. The current study is the first to demonstrate that CXCR5 signaling is critical for RPE cell homeostasis and is relevant for RD and AMD-like pathological changes. Our previous work demonstrated the essential roles of genetic CXCR5 deficiency in RPE defects and AMD-like pathologies in mice [17, 18].

Autophagy function is fundamental for RPE cells to degrade and recycle protein aggregates and damaged organelles, such as mitochondria. Our data have revealed the impaired function of autophagolysosomes in CXCR5-deficient RPE cells, as indicated by decreased L3B-II level and abnormal autophagosomes. Besides, we showed that $CXCR5^{-/-}$ RPE cells had

reduced degradation capacity mediated by lysosomes compared with the WT control cells using a reporter plasmid (GFP-LC3-RFP). Such a compromised autophagy function is likely associated with the increased cell toxicity and death observed for CXCR5$^{-/-}$ RPE cells when incubation with zymosan particles in cultures. In vivo, CXCR5$^{-/-}$ RPE cells contain increased mitochondrial markers and numbers with abnormal structures, reminiscent of the impaired mitophagy function (Fig. S4). It would be interesting to understand whether mitochondria become dysfunctional and contribute to the abnormalities of CXCR5$^{-/-}$ RPE cells, and thereby sub-RPE depositions.

Escalated protein abundance and nuclear localization of FOXO1 in CXCR5-deficient RPE suggest its transcription activation. Previous reports established FOXO1 presence in human RPE cells and its involvement in abnormal RPE function [28]. Therefore, FOXO1 inhibition may be a potential therapeutic solution to prevent RPE dysfunction and AMD development. To support this idea, our study showed that FOXO1 inhibitor AS1842856 can revert RPE ZO-1 degradation by CXCR5 deficiency. Whether FOXO1 inhibition can rescue the other defects of CXCR5$^{-/-}$ RPE cells, such as barrier impairment, autophagy deregulation, and the EMT, is to be elucidated.

In the present study, we demonstrate that CXCR5 is critical for RPE homeostasis. Expression of CXCR5 has been shown to consistently increase in the vitreous humor of AMD patients [16], suggesting its potential role in this pathology. There are certain similarities between CXCR5$^{-/-}$ mice and well-characterized Stargardt's Disease rodent model ABCA4 KO mice [29], both of which demonstrate slow RD, sub-RPE depositions, and eventual EMT [30]. However, while in ABCA4 KO mice, photoreceptor degeneration is associated with the impaired visual cycle proteins accumulation, CXCR5-deficient RPE demonstrates abnormalities while isolated in cell culture with no photoreceptor component present. Further study is required to elucidate the CXCR5 presence and function in photoreceptors cells. Interestingly, we also found that human RPE cells express CXCR5, and CRISPR/Cas9-mediated ablation of CXCR5 reproduce many of the current study findings in human RPE cells (research is ongoing), which suggests a potential role of CXCR5 in RPE dysfunction-related disorders, such as AMD. The extracellular deposition of β-amyloid and APOE by CXCR5-deficient RPE cells is consistent with our observation in aged CXCR5-deficient animals [18] and our recently developed CXCR5/NRF2 DKO animals that develop RD phenotype at the early adult age [19]. However, the phenomena were not observed or less severe in young single CXCR5 knockout animals, as indicated by the progression of EMT during aging (Fig. 5). The possible explanation is that the CXCR5$^{-/-}$ RPE are more susceptible to the retinal changes caused by age than the WT RPE, leading to RPE abnormalities and dysfunction. The additive effects of abnormal RPE and age-related changes, such as oxidative stress and inflammation, cause the RD and AMD-like phenotypes in aged CXCR5$^{-/-}$ mice, which are not present in the young animals.

In summary, the CXCR5 GPCR receptor signaling protein is required for RPE cell homeostasis. This particular deficiency affects RPE cells phenotype and function, leading to EMT, autophagy, dysfunction, and extracellular deposition. PI3K/AKT/FOXO1 is likely the underlying signal transduction pathway that mediates CXCR5's function in RPE.

Materials and methods

Animals

All animal experiments were approved by the University of Missouri Institutional Animal Care and Use Committee (Protocol number: 9520) and performed in accordance with the "Statement for the Use of Animals in Ophthalmic and Vision Research" of the Association for Research in Vision and Ophthalmology. The [B6.129S2(Cg)-CXCR5tm1$^{Lipp/J}$] (CXCR5, KO) and [C57BL/6J] (WT) mice strains were purchased from Jackson Laboratory. CXCR5 mice (https://www.jax.org/strain/006659) are obtained from a mixed C57/BL6J/N background with a predominance of the C57/BL6J genome. All mice were housed in the special pathogen-free animal facilities of the Bone Life Sciences Center at the University of Missouri and were fed normal chow diets and provided with water ad libitum. Genotyping was performed with the assistance of Transnetyx (Cordova, TN, USA) Outsourced PCR Genotyping Services (www.transnetyx.com). The animals were validated for knockout of the CXCR5 gene and the presence of neomycin resistance genes. All mice were screened for the presence of Rd8-associated nucleotide deletion on the Crumbs homolog 1 (CRB1) gene using the Rd8 genotyping probe designed by Transnetyx and based on our previous Sanger sequencing data from the 3600–3700 region of the CRB1 gene (canonical transcript M_133239) [18] and found to be Rd8 mutation-negative.

Imaging

Visible light images were acquired using the EVOS FL color and EVOS M7000 microscopes (Thermo Fisher Scientific, Waltham, MA, USA). Fluorescent images were obtained with a LeicaSP8 laser confocal microscope (Leica AG, Wetzlar, Germany).

Histological sections and 3,3′-diaminobenzidine (DAB) staining

Eyeballs were fixed with HistoChoice Molecular Biology fixative (H120–4L, VWR Life Science, Radnor, PA, USA) for 12 h and stored in PBS (10010023, Thermo Fisher Scientific) until the specimens were processed for paraffin embedding and sectioning (5-μm thick). The sections were rehydrated using gradations of xylene and ethanol. Heat-induced antigen retrieval was performed in a citrate buffer (pH: 6.0), and sections were depigmented in 10% H_2O_2 for 120 min at 65 °C [21]. The sections were then blocked with 5% bovine serum albumin (BSA; A7096) at RT for 1 h and then incubated with primary CXCR5 antibodies (Table 1) overnight at 4 °C. Following PBS-Tween 20 (0.05%; PBS-T) washing, horseradish peroxidase (HRP)-conjugated secondary antibody (1:1000; Biorad) was applied for 1 h. The CXCR5 signals were visualized by incubation with a working solution of the DAB substrate kit (34002; Thermo Fisher) for 7 min. The reaction was stopped by briefly washing the samples with PBS.

Lactate dehydrogenase assay in the RPE cell cultures

CXCR5 KO and C57BL6-WT RPE cells were cultured in 24-well plates until they reached confluence and maturation. Treatment with H_2O_2 (1 μM, 12 h) followed by an LDH assay (Thermo Fisher Scientific) of culture media to quantitatively evaluate the H_2O_2 toxicity; the kit was used according to the instruction manual, and the resulting absorbances were read

at 490 nm using an 800 TS Absorbance Reader (BioTek Instruments, Winooski, VT, USA). Absorbances at 650 nm were used as a reference wavelength.

Primary RPE cell cultures and treatments

Following mouse sacrifice by CO_2 inhalation, RPE cells were isolated from adult (6-month-old) C57BL6-WT mice and CXCR5 KO mice by careful dissection of the eye globe on ice and removal of the anterior chamber and retina. The eyecup was then incubated with trypsin Gibco™ Trypsin-ethylenediamine tetra-acetic acid (0.25%) for 40 min with the RPE cell layer facing down. Following the initial digestion, the RPE cells were released by gentle shaking of the eyecup with sterile forceps. The isolated RPE cells were cultured with an N1 complete medium on attachment factor (4Z0–201; Cell systems)-coated cell culture flasks and chamber slide Millicell EZ slides (Millipore, Billerica, MA, USA) according to the protocol described in the literature [31]. Briefly, N1 media was prepared in 500 ml of Minimum Essential Medium (MEM) Alpha (12571–063; Gibco) with 50 ml of fetal bovine serum, 5 ml of N1 media supplement (N6530; Sigma), 5 ml of GlutaMax-I (100x; 35050–061; Gibco), 5 ml of MEM non-essential amino acids (100x; M7145; Sigma), 6.5 μg of 3,3′,5-triiodo-L-thyronin (triiodothyronine; T5516; Sigma), 125 mg taurine (T0625; Sigma), 10 μg of hydrocortisone (H0888; Sigma), and 5 ml of penicillin-streptomycin. The RPE cells reached confluence and maturation at 4 weeks, as indicated by the robust expression of RPE65 and the lack of proliferation of the other cell types. WT RPE cells were treated with PBS (control), or H_2O_2 (1 μM, 12 h). For experiments involving inhibition of PI3K LY294002 (L9908–5MG; Sigma; 25 μM) and FOXO1 (34455–10MG; Millipore, Billerica, MA, USA; 0.1 μM) were used. Both inhibitors were dissolved in DMSO; an equal amount of DMSO was used in the treatment of control cells. In experiments involving stimulation of CXCR5 by its ligand CXCL13, carrier-free recombinant CXCL13 (583902; Biolegend) was used at 100 ng/ml concentration.

The RPE cells were grown on a cellulose matrix (aimed to imitate the Bruch's membrane) with a pore size of 0.45 μm (R9NA09917, Millicell, Merk Millipore) for 4 weeks in N1 media. The RPE cell culture on the porous substrate was carried out using a modification of the protocol described by Johnson et al. for primary human RPE [22].

Immunofluorescence staining

Primary mouse RPE cells were seeded onto Millicell EZ Slides (Millipore, Billerica, MA, USA) under the same experimental conditions as those for the TER and WB experiments. At the experimental endpoint, the samples were mildly fixed in 2% paraformaldehyde (VVR Life Science) for 10 min, permeabilized by incubation in 0.05% Triton X-100 for 10 min and blocked with 2.5% normal goat serum for 1 h at room temperature (RT). The samples were then incubated with primary antibodies (Table 1). After PBS-T washing, they were then visualized by goat anti-rabbit IgG (H + L), Cyanine5 (A10523, 1:1000; Thermo Fisher), goat anti-rabbit IgG (H + L), Alexa Fluor 488 (A-11034, 1:1000, Thermo Fisher), and goat anti-mouse IgG (H + L), Cyanine5 (A10524, 1:1000, Thermo Fisher). The cell nuclei were visualized by incubation with 4′,6-diamidino-2-phenylindole (DAPI); (1:5000; Sigma). The slides were mounted with a ProLong Diamond antifade reagent (Thermo Fisher).

Western blots and densitometry analysis

WB was performed as previously described with some modifications [32, 33]. Primary RPE cells grown in six-well plates were washed with cold PBS three times, detached with a cell scraper, and collected by centrifugation. The harvested cell pellets were sonicated in a cold radioimmunoprecipitation assay buffer containing FAST protease inhibitors (Cat#: S8830, Sigma). The protein concentration was determined using a Qubit 4 fluorometer (Thermo Fisher). Prior to the electrophoretic transfer to 0.45 μm pore size nitrocellulose membranes, 30–50 μg total protein per lane was separated by sodium dodecyl sulfate-polyacrylamide gel electrophoresis (4–20% polyacrylamide gel). The membranes were blocked with 5% BSA (A7096) at RT for 1 h and then incubated overnight at 4 °C with the primary antibodies (Table 1). After being washed with a PBS-T buffer, the blots were incubated with an HRP-conjugated secondary antibody (1:1000; Biorad) for 1 h at RT. The signals were developed with enhanced chemiluminescence with a SuperSignal West Pico kit (Thermo Fisher) and detected with an ImageQuant LAS 500 (GE Healthcare). The densitometric analysis of WBs was performed with ImageJ software (National Institute of Health, Bethesda, MD, USA) using positive membrane images. All the quantification results were averaged from three protein blots and expressed as the mean ratio of the values (target protein/housekeeping protein) ± standard deviation (SD).

RPE–choroid–sclera complex flat mounts

Mouse eyes from 6, 12, and 24 m.o. WT and KO animals were fixed and dissected, as reported previously [18]. Briefly, under a dissection microscope, the anterior segment tissues and vitreous were removed to produce an eyecup. The retina was then gently separated from the RCSC, and four relaxing radial incisions were made in the RCSC and retina in order to produce a flat-mount. The RCSC was blocked and permeabilized overnight with a solution composed of 2.5% BSA (A9467–100G, Sigma-Aldrich) in PBS with 0.01% Triton X; the RCSC samples were then incubated with primary antibodies to N-cadherin, αSMA, and vimentin (Table 1). Following washing and incubation for 24 h with goat anti-rabbit IgG (H + L), Cyanine5 (A10523, 1:1000; Thermo Fisher), goat anti-rabbit IgG (H + L), and Alexa Fluor 488 (A-11034, 1:1000, Thermo Fisher), the nuclei were counterstained with DAPI 1:5000 (Sigma-Aldrich). Samples were mounted on slides with the ProLong Diamond antifade reagent. Samples that were incubated with a blocking buffer (the primary antibody was omitted) followed by secondary antibody incubation were used to correct confocal settings for a non-specific background.

Transepithelial resistance measurement using an electrical cell-impedance sensing system

The primary RPE cells were seeded on an eight-well ECIS array cultureware plate (8W10E PET; Applied BioPhysics) and cultured, as described above. The TER was monitored with the ECIS system (Applied BioPhysics) in real-time. The changes in TER have been monitored automatically every 600 s at 4 kHz AC frequency and recorded by the ECIS software [34].

Transmission electron microscopy and scanning electron microscopy analysis

Unless stated otherwise, all electron microscopy (EM)-related reagents were purchased from Electron Microscopy Sciences. The KO and WT RPE cells were plated on cell culture-treated coverslips to ensure adhesion to the 24-well plates and were cultured for 4 weeks. The samples were fixed with an EM fixative solution in 2% paraformaldehyde and 2% glutaraldehyde in a 100-mM sodium cacodylate buffer with a pH of 7.35. Next, the fixed cells were rinsed with 100-mM sodium cacodylate buffer at a pH of 7.35 (Sigma-Aldrich, St. Louis, MO, USA) and 130 mM of sucrose. Secondary fixation was performed using 1% osmium tetroxide (Ted Pella, Inc., Redding, CA, USA) in a 2-ME buffer using a Pelco Biowave (Ted Pella, Inc., Redding, CA, USA) operated at 100 W for 1 min. The specimens were next incubated at 4 °C for 1 h and then rinsed first with a cacodylate buffer and then further using distilled water. En bloc staining was performed using 1% aqueous uranyl acetate and incubated at 4 °C overnight then rinsed with distilled water. Using the Pelco Biowave, a graded dehydration series (per exchange, 100 W for 40 s) was performed using ethanol and then transitioned into acetone, and the dehydrated specimens were then infiltrated with Epon resin (250 W for 3 min) and polymerized at 60 °C overnight. The sections were cut to a thickness of 75 nm using an ultramicrotome (Ultracut UCT, Leica Microsystems, Germany) and a diamond knife (Diatome, Hatfield, PA, USA). The images were acquired with a JEOL JEM 1400 transmission EM (JEOL, Peabody, MA, USA) at 80 kV on a Gatan Ultrascan 1000 CCD (Gatan, Inc, Pleasanton, CA, USA). For the SEM, the cells were cultured and fixed with the EM fixative as described above. Secondary fixation was performed using 1% osmium tetroxide (Ted Pella, Inc. Redding, CA, USA) in a cacodylate buffer using a Pelco Biowave (Ted Pella, Inc. Redding, CA, USA) operated at 100 W for 1 min. The specimens were next incubated at 4 °C for 1 h and then rinsed first with a cacodylate buffer and then further with distilled water. Using the Pelco Biowave, a graded dehydration series (per exchange, 100 W for 40 s) was performed using ethanol. The samples were dried using the Tousimis Autosamdri 815 (Tousimis, Rockville, MD, USA), and the samples were sputter-coated with 5 nm of platinum using the EMS 150T-ES Sputter Coater. The images were acquired with an FEI Quanta 600F SEM (FEI, Hillsboro, OR, USA) at a voltage of 5.0 kV and a working distance of 8.3 mm (Everhart-Thornley Detector).

Autophagy probe GFP-LC3-RFP-LC3ΔG

An autophagic flux probe GFP-LC3-RFP-LC3ΔG (Addgene; plasmid #84573) [24] was transfected to mouse WT and KO primary RPE cells using lipofectamine 3000 transfection kit (Thermo Fisher). Briefly, 3 μl lipofectamine 3000 (100022052, Thermo Fisher) was diluted in 250 μl Opti-MEM (Gibco). The reagent P3000 (100022058; Thermo Fisher) was diluted in 250 μl Opti-MEM (Gibco), and 1 μg of GFP-LC3-RFP-LC3ΔG DNA was combined with reagent P3000. The transfection efficacy in mouse primary RPE cells was established by transfection of different amounts (0.1–5 μg) of pEF-GFP (Addgene; plasmid #11154 [35]; Data not shown). The solutions were combined and following 10 min incubation was added to RPE cells, following overnight incubation Opti-MEM was replaced with N1 media. The fluorescent GFP and RFP signals in live-cell cultures were detected using with a LeicaSP8 laser confocal microscope the fluorescence intensity was quantified

using ImageJ to determine GPF to RFP fluorescence ratio by dividing GFP intensity values to RFP.

Zymosan bioparticles phagocytosis

pHrodo™ Green Zymosan Bioparticles™ conjugate (P35365; Thermo Fisher) was dissolved according to the instruction manual, and 100 μg/ml was added to WT and KO primary mouse RPE cells. Following 24 h incubation, cells were washed with PBS and provided with new N1 media and cultured for another 24 h. PI (P3566; Thermo Fisher; 1:3000 dilution) was added to culture media 10 min before imaging.

BrdU incorporation ELISA assay

The WT mouse primary RPE cells were seeded in 96-well plates and cultured overnight in 100 μl N1 media. Then CXCL13 (100 ng/ml) or CXCL13 (100 ng/ml) with PI3K inhibitor LY294002 (L9908–5MG; Sigma; 25 μM) were added to N1 media. Control cells received equal amounts of PBS and DMSO. BrdU Cell Proliferation ELISA Assay Kit (6813, Cell Signalling Technology, Denvers, MA, USA) was used to evaluate the proliferation activity according to the manufacturer's instructions. The 450 nm absorbance was detected using an 800 TS Absorbance Reader (BioTek Instruments, Winooski, VT, USA).

Extracellular deposition analysis

The RPE cells isolated from the eyes of CXCR5 KO mice and WT-control mice were seeded and cultured on a cellulose matrix with a pore size of 0.45 μm (R9NA09917, Millicell, Merk Millipore) for 4 weeks in complete N1 media. Before the fixation, the RPE cell cytoplasm was tagged with calcein AM (Thermo Fisher; C1430; 1 μg/ml) in culture for 30 min. Cels were fixed in 2% paraformaldehyde (VVR Life Science) for 10 min and blocked with 2.5% normal goat serum for 1 h at RT. Cells were fixed with, blocked with BSA as described above, and incubated overnight at 4 °C with β-amyloid and APOE antibodies (Table 1), followed by detection with Cy5 conjugated anti-rabbit (A10523, 1:1000; Thermo Fisher) and anti-goat (ab6566; 1:1000; Abcam) secondary antibody. Following washing with PBS-T three times for 15 min, membranes were embedded in OCT compound snap-frozen using liquid nitrogen-cooled isopropanol, and 5 μm cross-sections were prepared. The resulting samples were mounted with ProLong Diamond antifade reagent and imaged.

Dot immunoblotting

Modification of the Dot immunoblotting assay [36] was used to detect the extracellular presence of CXCL13. N1 culture media (5 μl) conditioned by 3 days culture with primary mouse RPE cells and 5 μl of culture media without cultured cells (control) were supplemented with FAST protease inhibitors (Cat#: S8830, Sigma) 1:100 and deposited on a dry nitrocellulose membrane (Bio-Rad). Following 15 min incubation at RT, the total protein deposition was visualized by the incubation with Pierce™ Reversible Protein Stain Kit (24580; Thermo Fisher Scientific, Waltham, MA, USA). The membranes were then washed with PBS and blocked with 2.5% BSA (A7096, Sigma-Aldrich, St Louis, MO, USA) in PBS at RT for 1 h and then incubated overnight at 4 °C with CXCL13 antibody (Table 1). The membrane was washed three times for 5 min with PBS-T (0.05% Triton) and incubated with

HRP-conjugated secondary antibody (1:1000; Biorad) for 1 h at RT. Following additional washing, signals were developed with ECL using a Super Signal West Pico Kit (Thermo Fisher Scientific) and detected with ImageQuant LAS 500 (GE Healthcare).

Statistical analysis

All experiments were performed in triplicate. Experimental values were expressed as the mean ± SD for the respective groups. Statistical analyses were performed with GraphPad Prism software (https://www.graphpad.com/scientific-software/prism/). The Student's *t* test was used for the comparison of the two groups, and one-way analysis of variance with Tukey multiple comparisons was used whenever comparing multiple groups. A p value of <0.05 was considered statistically significant. The following designations for the p value were used in the manuscript figures: n.s. $p > 0.05$; *$p < 0.05$; **$p < 0.01$; ***$p < 0.00.1$.

Supplementary Material

Refer to Web version on PubMed Central for supplementary material.

Acknowledgements

The authors would like to acknowledge the following contributors: Allen Raye (University of Missouri Department of Biomedical Sciences, Columbia, Missouri, USA) for assistance with animal resources; DeAna Grant Electron Microscopy core (University of Missouri, Columbia, Missouri, USA) for technical assistance with EM data acquisition. Ms. Lijuan Fan (Department of Ophthalmology, University of Missouri School of Medicine, Columbia, Missouri) for benchwork assistance. Ms. Catherine Brooks J. (Department of Ophthalmology, University of Missouri School of Medicine, Columbia, Missouri) for benchwork assistance and language corrections. Confocal images were acquired at the University of Missouri Molecular Cytology Core facility (University of Missouri, Columbia, Missouri, USA).

Funding

HH's research was supported by NIH grant R01 EY027824 and Missouri University start-up funds. The content is solely the responsibility of the authors and does not necessarily represent the official views of the National Institutes of Health.

Data availability

All data generated and analyzed in the current study are included in this published article and its Supplementary information.

References

1. Kaneko H, Dridi S, Tarallo V, Gelfand BD, Fowler BJ, Cho WG, et al. DICER1 deficit induces Alu RNA toxicity in age-related macular degeneration. Nature. 2011;471:325–30. [PubMed: 21297615]
2. Kerur N, Fukuda S, Banerjee D, Kim Y, Fu D, Apicella I, et al. cGAS drives noncanonical-inflammasome activation in age-related macular degeneration. Nat Med. 2018;24:50–61. [PubMed: 29176737]
3. Ma W, Yan RT, Li X, Wang SZ. Reprogramming retinal pigment epithelium to differentiate toward retinal neurons with Sox2. Stem Cells. 2009;27:1376–87. [PubMed: 19489100]
4. Zhao C, Yasumura D, Li X, Matthes M, Lloyd M, Nielsen G, et al. mTOR-mediated dedifferentiation of the retinal pigment epithelium initiates photoreceptor degeneration in mice. J Clin Invest. 2011;121:369–83. [PubMed: 21135502]

5. Brown EE, DeWeerd AJ, Ildefonso CJ, Lewin AS, Ash JD. Mitochondrial oxidative stress in the retinal pigment epithelium (RPE) led to metabolic dysfunction in both the RPE and retinal photoreceptors. Redox Biol. 2019;24:101201. [PubMed: 31039480]
6. Esteve-Rudd J, Hazim RA, Diemer T, Paniagua AE, Volland S, Umapathy A, et al. Defective phagosome motility and degradation in cell nonautonomous RPE pathogenesis of a dominant macular degeneration. Proc Natl Acad Sci USA. 2018;115:5468–73. [PubMed: 29735674]
7. Golestaneh N, Chu Y, Xiao YY, Stoleru GL, Theos AC. Dysfunctional autophagy in RPE, a contributing factor in age-related macular degeneration. Cell Death Dis. 2017;8:e2537. [PubMed: 28055007]
8. Dobner T, Wolf I, Emrich T, Lipp M. Differentiation-specific expression of a novel G protein-coupled receptor from Burkitt's lymphoma. Eur J Immunol. 1992;22:2795–9. [PubMed: 1425907]
9. Kazanietz MG, Durando M, Cooke M. CXCL13 and Its ReceptorCXCR5 in Cancer: inflammation, immune response, and beyond. Front Endocrinol (Lausanne). 2019;10:471. [PubMed: 31354634]
10. Chevalier N, Jarrossay D, Ho E, Avery DT, Ma CS, Yu D, et al. .CXCR5 expressing human central memory CD4 T cells and their relevance for humoral immune responses. J Immunol. 2011;186:5556–68. [PubMed: 21471443]
11. Xiao H, Luo G, Son H, Zhou Y, Zheng W. Upregulation of peripheral CD4+CXCR5+ T cells in osteosarcoma. Tumour Biol. 2014;35:5273–9. [PubMed: 24519063]
12. Yan Q, Yuan Y, Yankui L, Jingjie F, Linfang J, Yong P, et al. The expression and significance of CXCR5 and MMP-13 in colorectal cancer. Cell Biochem Biophys. 2015;73:253–9. [PubMed: 25726157]
13. Mitkin NA, Hook CD, Schwartz AM, Biswas S, Kochetkov DV, Muratova AM, et al. p53-dependent expression of CXCR5 chemokine receptor in MCF-7 breast cancer cells. Sci Rep. 2015;5:9330. [PubMed: 25786345]
14. Zhang X, Huang W, Chen X, Lian Y, Wang J, Cai C, et al. .CXCR5-overexpressing mesenchymal stromal cells exhibit enhanced homing and can decrease contact hypersensitivity. Mol Ther. 2017;25:1434–47. [PubMed: 28454789]
15. Ma W, Cojocaru R, Gotoh N, Gieser L, Villasmil R, Cogliati T, et al. Gene expression changes in aging retinal microglia: relationship to microglial support functions and regulation of activation. Neurobiol Aging. 2013;34:2310–21. [PubMed: 23608111]
16. Spindler J, Zandi S, Pfister IB, Gerhardt C, Garweg JG. Cytokine profiles in the aqueous humor and serum of patients with dry and treated wet age-related macular degeneration. PLoS ONE. 2018;13:e0203337. [PubMed: 30157273]
17. Huang H, Liu Y, Wang L, Li W. Age-related macular degeneration phenotypes are associated with increased tumor necrosis-alpha and subretinal immune cells in aged Cxcr5 knockout mice. PLoS ONE. 2017;12:e0173716. [PubMed: 28282423]
18. Lennikov A, Saddala MS, Mukwaya A, Tang S, Huang H. Autoimmune-mediated retinopathy in CXCR5-deficient mice as the result of age-related macular degeneration associated proteins accumulation. Front Immunol. 2019;10:1903. [PubMed: 31474986]
19. Huang H, Lennikov A. CXCR5/NRF2 double knockout mice develop retinal degeneration phenotype at early adult age. Exp Eye Res. 2020;196:108061. [PubMed: 32387618]
20. Saddala MS, Lennikov A, Mukwaya A, Huang H. Transcriptome-wide analysis of CXCR5 deficient retinal pigment epithelial (RPE) cells reveals molecular signatures of RPE homeostasis. Biomedicines. 2020;8:147–19. [PubMed: 32492870]
21. Manicam C, Pitz S, Brochhausen C, Grus FH, Pfeiffer N, Gericke A. Effective melanin depigmentation of human and murine ocular tissues: an improved method for paraffin and frozen sections. PLoS ONE. 2014;9:e102512. [PubMed: 25025426]
22. Johnson LV, Forest DL, Banna CD, Radeke CM, Maloney MA, Hu J, et al. Cell culture model that mimics drusen formation and triggers complement activation associated with age-related macular degeneration. Proc Natl Acad Sci USA. 2011;108:18277–82. [PubMed: 21969589]
23. Barth S, Glick D, Macleod KF. Autophagy: assays and artifacts. J Pathol. 2010;221:117–24. [PubMed: 20225337]
24. Kaizuka T, Morishita H, Hama Y, Tsukamoto S, Matsui T, Toyota Y, et al. An autophagic flux probe that releases an internal control. Mol Cell. 2016;64:835–49. [PubMed: 27818143]

25. Yamamoto H, Itoh N, Kawano S, Yatsukawa Y-i, Momose T, Makio T, et al. Dual role of the receptor Tom20 in specificity and efficiency of protein import into mitochondria. Proc Natl Acad Sci USA. 2011;108:91–6. [PubMed: 21173275]
26. Tzivion G, Dobson M, Ramakrishnan G. FoxO transcription factors; regulation by AKT and 14–3-3 proteins. Biochim Biophys Acta. 2011;1813:1938–45. [PubMed: 21708191]
27. Cao X, Li W, Liu Y, Huang H, Ye CH. The anti-inflammatory effects of CXCR5 in the mice retina following ischemia-reperfusion injury. Biomed Res Int. 2019;2019:3487607. [PubMed: 31355256]
28. Busch C, Annamalai B, Abdusalamova K, Reichhart N, Huber C, Lin Y, et al. Anaphylatoxins activate Ca(2+), Akt/PI3-Kinase, and FOXO1/FoxP3 in the retinal pigment epithelium. Front Immunol. 2017;8:703. [PubMed: 28663750]
29. Weng J, Mata NL, Azarian SM, Tzekov RT, Birch DG, Travis GH. Insights into the function of rim protein in photoreceptors and etiology of stargardt's disease from the phenotype in abcr knockout mice. Cell. 1999;98:13–23. [PubMed: 10412977]
30. Zhou M, Geathers JS, Grillo SL, Weber SR, Wang W, Zhao Y, et al. Role of epithelial-mesenchymal transition in retinal pigment epithelium dysfunction. Front Cell Dev Biol. 2020;8:501–13. [PubMed: 32671066]
31. Fernandez-Godino R, Garland DL, Pierce EA. Isolation, culture and characterization of primary mouse RPE cells. Nat Protoc. 2016;11:1206–18. [PubMed: 27281648]
32. Huang H, Shen J, Vinores SA. Blockade of VEGFR1 and 2 suppresses pathological angiogenesis and vascular leakage in the eye. PLoS ONE. 2011;6:e21411. [PubMed: 21731737]
33. Huang H, Van de Veire S, Dalal M, Parlier R, Semba RD, Carmeliet P, et al. Reduced retinal neovascularization, vascular permeability, and apoptosis in ischemic retinopathy in the absence of prolyl hydroxylase-1 due to the prevention of hyperoxia-induced vascular obliteration. Invest Ophthalmol Vis Sci. 2011;52:7565–73. [PubMed: 21873682]
34. Giaever I, Keese CR. Micromotion of mammalian cells measured electrically. Proc Natl Acad Sci USA. 1991;88:7896–900. [PubMed: 1881923]
35. Matsuda T, Cepko CL. Electroporation and RNA interference in the rodent retina in vivo and in vitro. Proc Natl Acad Sci USA. 2004;101:16–22. [PubMed: 14603031]
36. Huang H, Lennikov A, Saddala MS, Gozal D, Grab DJ, Khalyfa A, et al. Placental growth factor negatively regulates retinal endothelial cell barrier function through suppression of glucose-6-phosphate dehydrogenase and antioxidant defense systems. FASEB J. 2019;33:13695–709. [PubMed: 31585507]

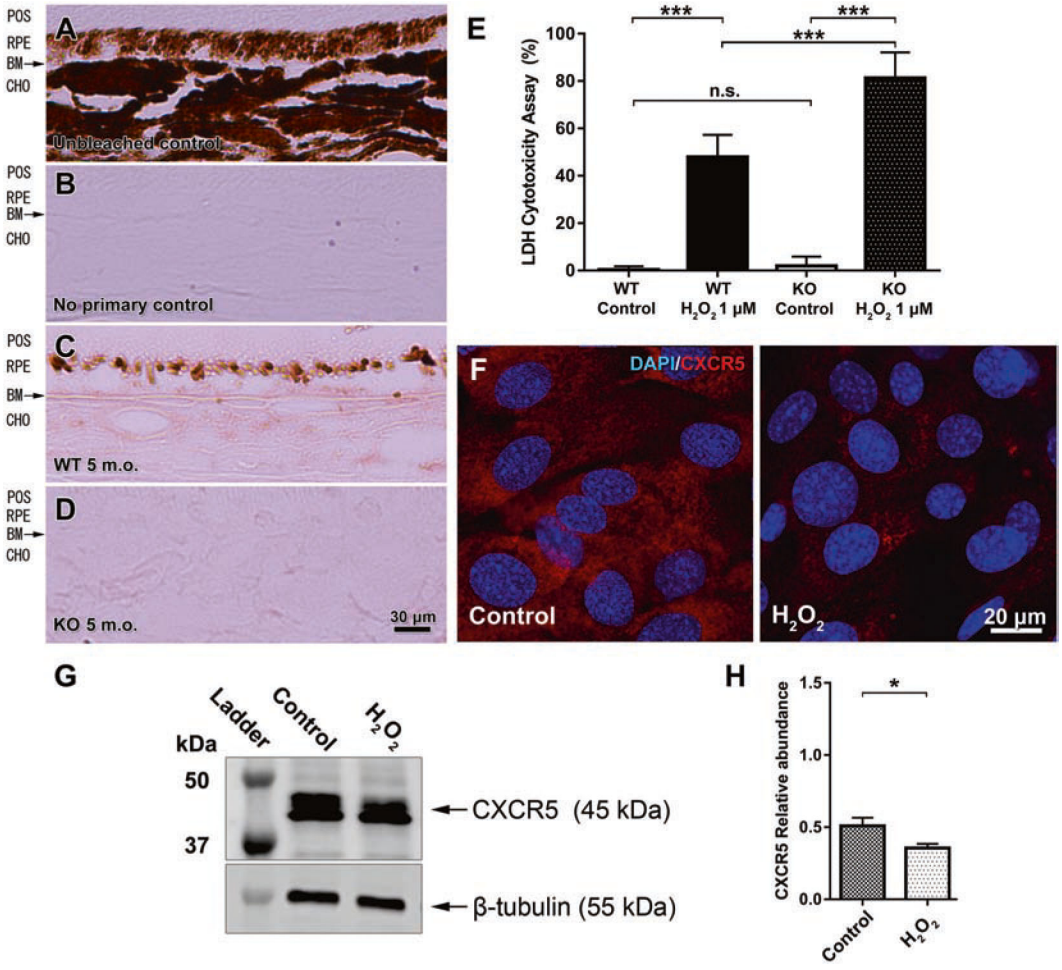

Fig. 1. CXCR5 expression in mouse RPE cells is reduced by oxidative stress environment.

(a) Paraffin section of mouse eye was rehydrated, but unstained, representing native pigmentation of an adult C57BL6 (WT) RPE and choroid. (**b**) DAB staining of H_2O_2 bleached WT eye cross-section with the primary antibody omitted demonstrates complete elimination of native pigmentation and a lack of non-specific binding of the secondary antibody (specificity control). (**c**) DAB staining of CXCR5 in the WT mouse eye visualizes signals from the RPE cell layer and weakly from the choroid. (**d**) Adult $CXCR5^{-/-}$ (KO) mouse eye section, which is bleached with H_2O_2 and incubated with CXCR5 primary antibodies, demonstrates no specific signals (KO control). POS photoreceptor outer segments, RPE retinal pigment epithelium, BM Bruch's membrane, CHO choroid. Immunofluorescent results are shown in Fig. S1. (**e**) LDH-cytotoxicity assay in primary RPE cells isolated from $CXCR5^{-/-}$ KO and WT mice and treated with H_2O_2 1 μM for 12 h; the PBS treatment was used as the control. p values were denoted as follows; n.s. $p > 0.05$; *** $p < 0.01$ ($n = 8$). (**f**) Immunofluorescent detection of CXCR5 in primary mouse RPE cells isolated from WT mice and treated with PBS (control) or H_2O_2 1 μM for 12 h. The nuclei were counterstained with DAPI. (**g**) Representative western blot (WB) results of cell lysates obtained from WT primary mouse RPE cells that underwent the same treatment described above. β-tubulin used as the loading control; (**h**) densitometry analysis of WB in

the PBS-treated control and H_2O_2 1 μM treatment for 12 h. ($n = 3$). p values were denoted as follows: n.s. $p > 0.05$; *$p < 0.05$; **$p < 0.01$, and error bars represent the SD.

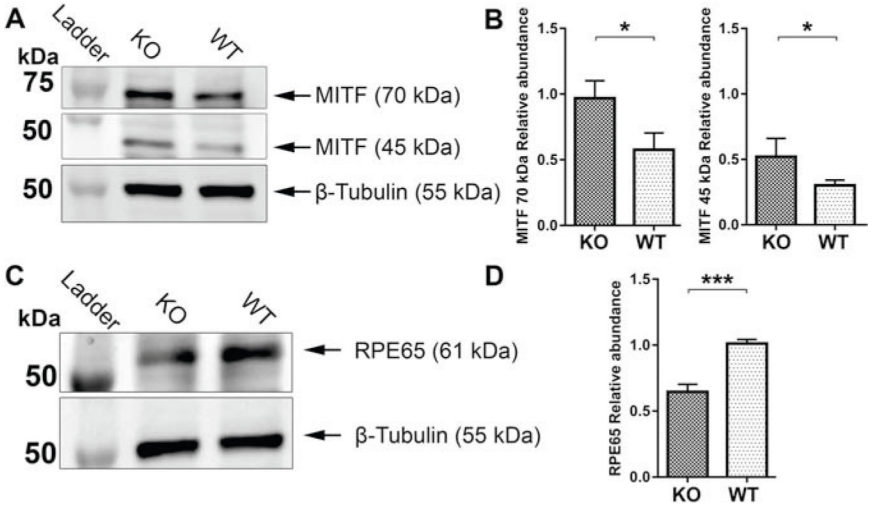

Fig. 2. De-differentiation of the primary CXCR5-deficient RPE cells.

Representative western blot results of MITF 45 kDa and 70 kDa isoforms (**a**) and densitometry analysis of the MITF blots (**b**); RPE65 (**c**) and densitometry analysis of the RPE65 blots (**d**) in cell lysates obtained from KO and WT primary mouse RPE. β-tubulin used as the loading control; ($n = 3$). p values were denoted as follows: n.s. $p > 0.05$; *$p < 0.05$; **$p < 0.01$, and error bars represent the SD.

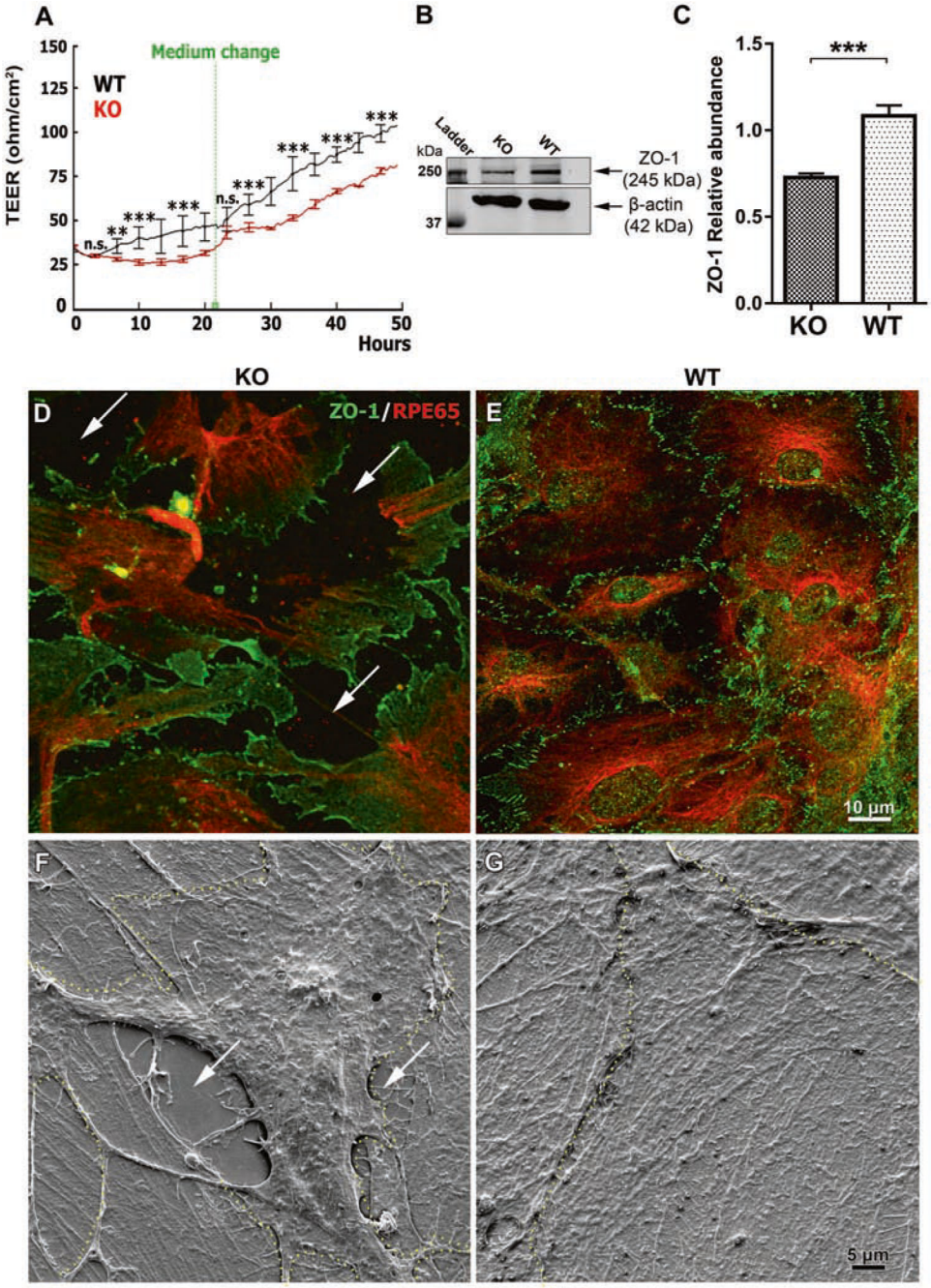

Fig. 3. The impaired barrier function of the CXCR5-deficient RPE cells.

(**a**) Transepithelial electrical resistance measurement in primary mouse RPE cells isolated from CXCR5$^{-/-}$ (KO; red) or WT (black) ($n = 8$). p values were denoted as follows: n.s. $p > 0.05$; ** $p < 0.01$; *** $p < 0.01$. Representative Western blot results (**b**) and quantitative analysis (**c**) of ZO-1 expression in KO and WT primary mouse RPE cell lysates. β-actin was used as the loading control ($n = 3$); p value was denoted: *** $p < 0.001$. Error bars represent the SD. Immunofluorescent double staining of ZO-1 and RPE65 in CXCR5-deficient RPE (**d**) and WT RPE (**e**) cells grown on supporting cellulose substrate. White arrows indicate voids between the cells. Scanning electron microscopy images of the cell-to-cell interface in

the KO (**f**) and WT (**g**) primary RPE cell monolayer. Note the broken junction connections and empty voids (white arrows) in KO, but the integral injunctions in WT, yellow dotted plots indicate the cell edges.

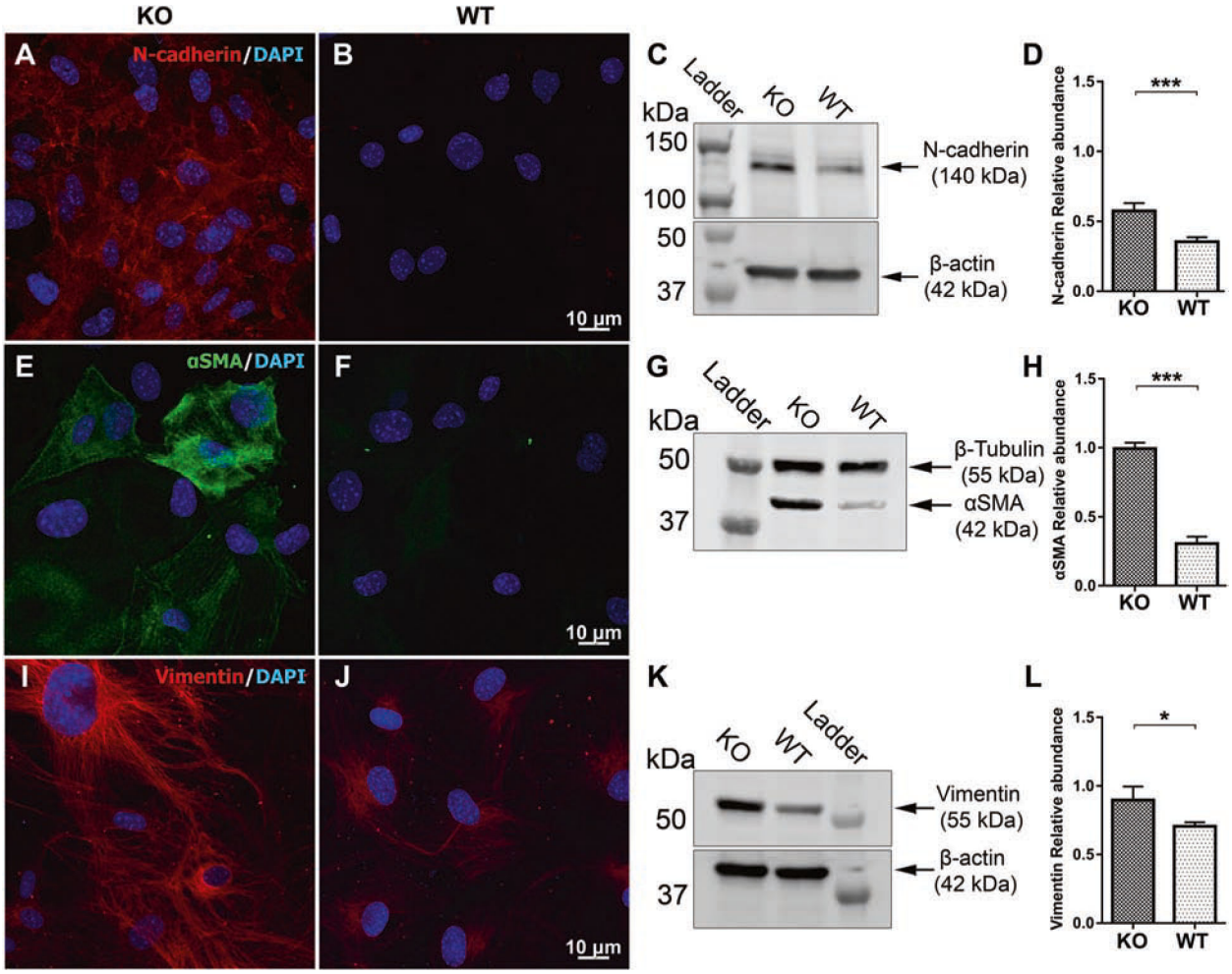

Fig. 4. Increased EMT markers in CXCR5-deficient RPE cells.

Immunofluorescent detection, representative western blot results, and quantitative analysis of N-cadherin (**a–d**), α-smooth muscle actin (αSMA; **e–h**), and vimentin (**i–l**) in primary mouse RPE cells isolated from CXCR5$^{-/-}$ KO and WT mice. Nuclei counterstained with DAPI. β-actin and β-tubulin were used as the loading control; *p* value was denoted as follows: $^{**}p < 0.01$; $^{***}p < 0.001$ ($n = 3$), and error bars represent the SD.

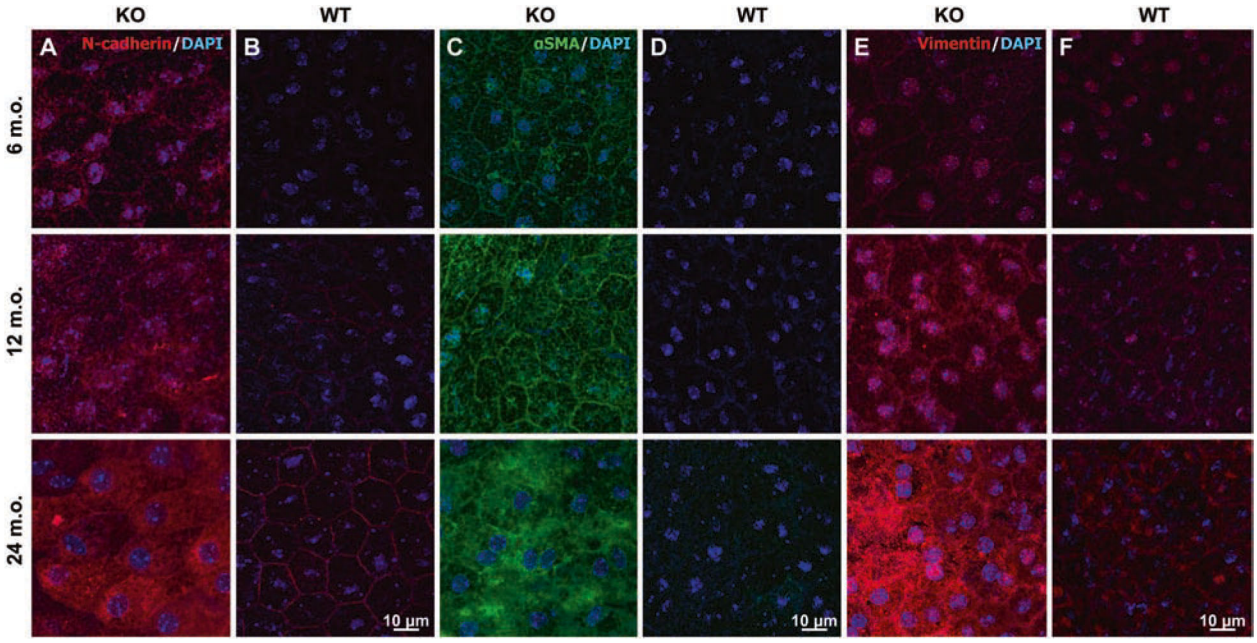

Fig. 5. Increased EMT markers in the CXCR5 KO mice with age.

Immunofluorescent staining of N-cadherin (**a, b**); αSMA (**c, d**); Vimentin (**e, f**) in RPE/choroid/scleral complexes of 6, 12, and 24-month-old CXCR5$^{-/-}$ KO and WT mice.

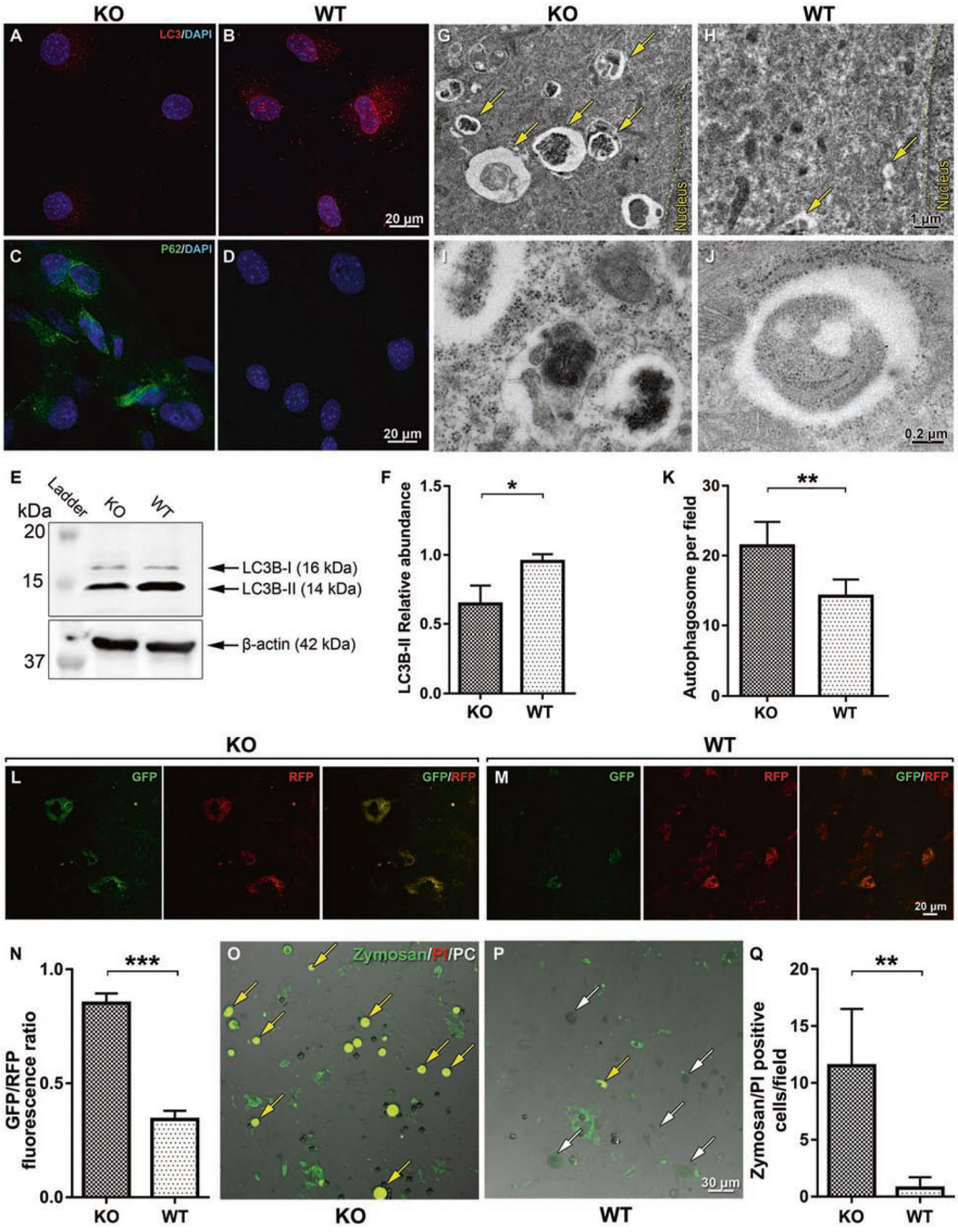

Fig. 6. Deregulated autophagy function of the CXCR5-deficient RPE cells.

Immunofluorescent detection of bulk LC3B (**a, b**) and P62 (**c, d**) in KO and WT primary RPE cells. Nuclei were counterstained with DAPI. Representative Western blot results (**e**) and quantitative analysis of LC3B-II (**f**) in the lysates from CXCR5$^{-/-}$ KO and WT RPE cells. β-actin was used as the loading control. *p* value was denoted as follows: *$p < 0.05$ ($n = 3$). Representative transmission electron microscopy (TEM) images of phagolysosomes (yellow arrows) in the cytoplasm of CXCR5$^{-/-}$ KO (**g**) and WT (**h**) RPE cells in the perinuclear area. The yellow dotted line designates the nuclear membrane. High

magnification (×10,000) of the phagolysosome vesicles in KO (**i**) and WT (**j**) primary mouse RPE cells indicates lead staining positive content (dark gray) within the phagolysosomes of KO RPE cells. **k** Quantitative analysis of the autophagolysosome numbers per field at ×800 magnification. *p* value was denoted as follows: $^{**}p < 0.01$ ($n = 5$). Autophagy flux analysis by transfection of KO (**l**) and WT (**m**) RPE cells with GFP-LC3-RFP-LC3ΔG 24 h after transfection. **n** Quantitative analysis of the fluorescent ratio between GFP/RFP signals. *p* value was denoted as follows: $^{*}p < 0.05$ ($n = 8$). Incubation of pHrodo Green Zymosan bioparticles conjugate (green) with KO (**o**) and WT (**p**) RPE cells 48 h after the introduction of bioparticles, cell death indicated by PI staining. Yellow arrows indicate dead cells strongly positive for zymosan signal. White arrows indicate PI-negative cells with decreased fluorescence and structural integrity of zymosan bioparticles. **q** Quantitative analysis of double-positive cells for zymosan and PI signals.

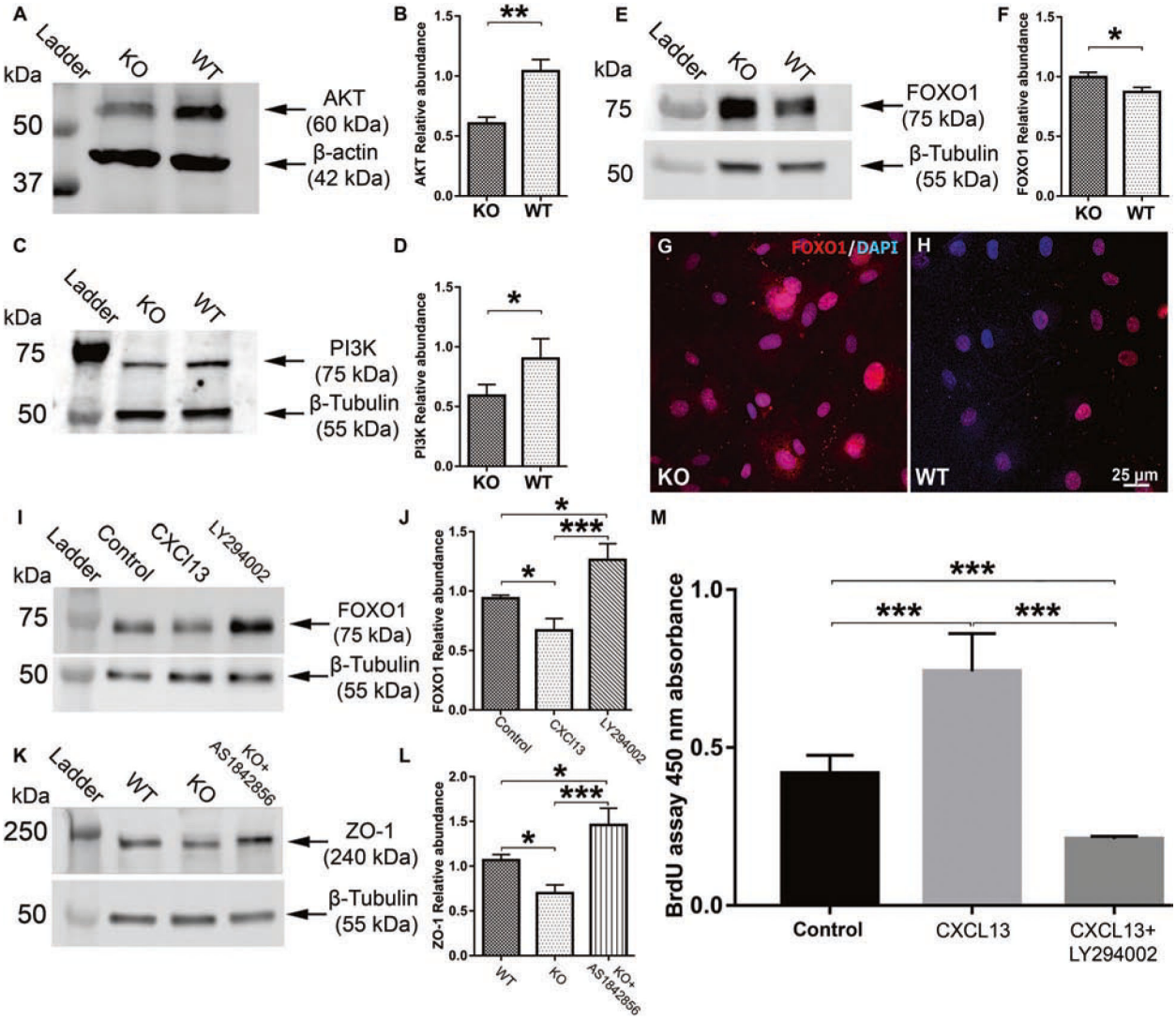

Fig. 7. PI3K-AKT-FOXO1 signaling in CXCR5-deficient RPE cells.

Representative western blot results, and quantitative analysis of AKT (**a, b**), PI3K (**c, d**), and FOXO1 (**e, f**) in primary mouse RPE cell lysates isolated from CXCR5$^{-/-}$ KO and WT mice. β-actin and β-tubulin were used as loading control. *p* value was denoted as follows: *$p < 0.05$; **$p < 0.01$ ($n = 3$), and error bars represent the SD. Immunofluorescent detection of FOXO1 in primary mouse RPE cells isolated from CXCR5$^{-/-}$ KO (**g**) and WT (**h**) mice. The nuclei were counterstained with DAPI. Western blot results (**i**) and quantification (**j**) of the FOXO1 expression in WT primary RPE cells treated with recombinant mouse CXCL13 (100 ng/ml) and LY294002 (25 μM). ZO-1 expression (**k**) and quantative analysis (**l**) of KO RPE cells treated with AS1842856 (0.1 μM), WT and KO RPE treated with DMSO were used as controls. β-tubulin were used as loading control. *p* value was denoted as follows: *$p < 0.05$; **$p < 0.01$ ($n = 3$). (**m**) Evaluation of RPE cells proliferation in WT RPE treated with recombinant mouse CXCL13 (100 ng/ml) and LY294002 (25 μM).

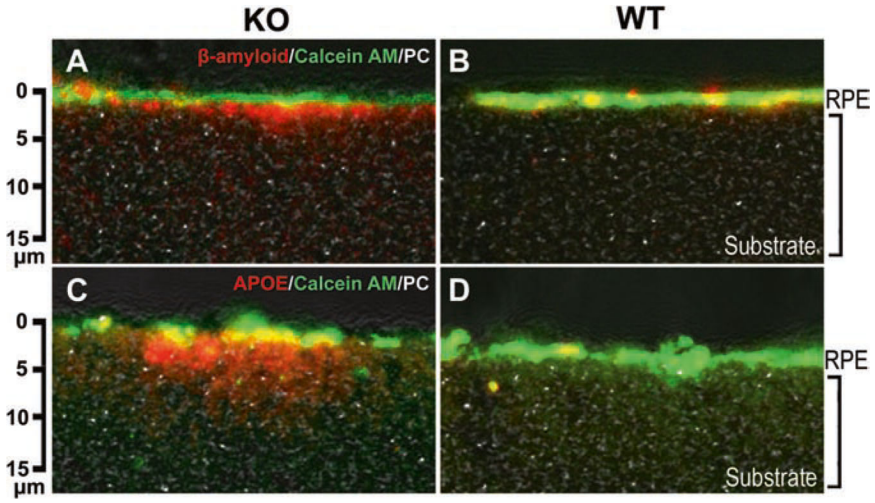

Fig. 8. Extracellular deposition of β-amyloid and APOE of primary mouse CXCR5 KO RPE cells.

Extracellular deposition in at a depth of 3–5 μm in WT and CXCR5 KO RPE cells of β-amyloid (**a, b**) and APOE (**c, d**). The cell cytoplasm is visualized by Calcein AM. The cellulose substrate is visualized by phase-contrast microscopy.

Table 1

A list of primary antibodies and dilutions used in the study.

Target protein	Produced by	Catalog number	Host	IHC dilution	WB dilution
CXCR5	Abcam	ab133706	Rabbit	1:100	1:1000
RPE65	Thermo Fisher	MA1–16578	Mouse	1:50	1:1000
ZO-1	Thermo Fisher	61–7300	Rabbit	1:100	1:1000
β-tubulin	Thermo Fisher	MA5–16038	Mouse	1:200	1:4000
MITF	Santa Cruz Bio	sc-25386	Rabbit	1:100	1:1000
N-cadherin	Thermo Fisher	33–3900	Mouse	1:100	1:1000
β-actin	Thermo Fisher	MA5–15739	Mouse	1:200	1:2000
αSMA	Thermo Fisher	MA5–11544	Mouse	1:100	1:1000
Vimentin	Thermo Fisher	PA5–27231	Rabbit	1:100	1:1000
LC3B	Cell Signaling	2775	Rabbit	1:50	1:1000
SQSTM1/p62	Cell Signaling	88588	Mouse	1:50	1:500
PI3K	Cell Signaling	4292	Rabbit	1:100	1:1000
AKT	Cell Signaling	4H10	Mouse	1:100	1:1000
FOXO1	Thermo Fisher	MA5–14846	Rabbit	1:100	1:1000
β-amyloid	Thermo Fisher	36–6900	Rabbit	1:100	1:1000
APOE	MilliporeSigma	AB947	Goat	1:50	1:1000
CXCL13	Thermo Fisher	PA5–47018	Rabbit	1:100	1:500